RESEARCH ARTICLE

Key Points:
- Validated microwave radiometer measured humidity with collocated GPS data
- Multiyear analysis of humidity variability over a tropical coastal station
- Vertical variability of humidity and its impact on Indian summer monsoon

Correspondence to:
C. Suresh Raju,
c_sureshraju@vssc.gov.in

Microwave radiometer observations of interannual water vapor variability and vertical structure over a tropical station

R. Renju[1], C. Suresh Raju[1], Nizy Mathew[1], Tinu Antony[1], and K. Krishna Moorthy[2]

[1]Space Physics Laboratory, Vikram Sarabhai Space Centre, Thiruvananthapuram, India, [2]ISRO Headquarters, Bengaluru, India

Abstract The intraseasonal and interannual characteristics and the vertical distribution of atmospheric water vapor from the tropical coastal station Thiruvananthapuram (TVM) located in the southwestern region of the Indian Peninsula are examined from continuous multiyear, multifrequency microwave radiometer profiler (MRP) measurements. The accuracy of MRP for precipitable water vapor (PWV) estimation, particularly during a prolonged monsoon period, has been demonstrated by comparing with the PWV derived from collocated GPS measurements based on regression model between PWV and GPS wet delay component which has been developed for TVM station. Large diurnal and intraseasonal variations of PWV are observed during winter and premonsoon seasons. There is large interannual PWV variability during premonsoon, owing to frequent local convection and summer thunderstorms. During monsoon period, low interannual PWV variability is attributed to the persistent wind from the ocean which brings moisture to this coastal station. However, significant interannual humidity variability is seen at 2 to 6 km altitude, which is linked to the monsoon strength over the station. Prior to monsoon onset over the station, the specific humidity increases up to 5–10 g/kg in the altitude region above 5 km and remains consistently so throughout the active spells.

1. Introduction

Water vapor plays a major role in many of the atmospheric and geophysical phenomena that include exchange of energy, radiation budget, formation of clouds, and weather systems, besides being a major greenhouse agent. The feedback through water vapor significantly amplifies the response of the climate system to changes in anthropogenic greenhouse gases such as carbon dioxide [*Held and Soden*, 2000]. Water vapor exchanges energy in the form of latent heat during evaporation and condensation, and it has significant role in cloud formation and convective activities. Hence, the information of its vertical distribution in the atmosphere and its temporal variability is essential in understanding regional weather as well as global climate.

The diurnal variation in water vapor affects the surface and atmospheric long-wave radiation and absorption of solar radiation, besides its effect on tropospheric correction in GPS-based positioning. It is also related to diurnal variation in convection, precipitation, surface wind convergence, and surface evapotranspiration [*Dai and Deser*, 1999]. The diurnal variation in water vapor studied using Global Positioning System (GPS) measurements and radiosonde data over 54 stations in North America have shown that most of the stations are characterized by significant diurnal variations [*Dai et al.*, 2002]. *Ohtani* [2001] investigated the correlation between diurnal cycle of rainfall and GPS-derived precipitable water vapor around the central part of the main island of Japan.

Precipitable water vapor (PWV), which is the height of the liquid water column when the entire water vapor in a vertical column of the atmosphere is condensed to liquid [*Parameswaran and Murthy*, 1990], represents the availability of the water vapor in the atmosphere. Weather forecast models demand water vapor information with high temporal resolution over a wide geographical region. Satellite measurements enable to construct global distribution of PWV [*Smith*, 1991], but with low temporal resolution, and are inadequate to resolve its large variability in short spatial and temporal scales. To address such limitations, a wide range of ground-based measurement techniques are there which include radiosondes, Sun photometry, Raman lidar systems, Fourier transform spectrometers, microwave radiometers, and GPS receivers [*Pérez-Ramírez et al.*, 2014].

Remote sensing techniques have the potential to monitor the temporal and spatial variations of water vapor continuously over a global scale. The water vapor estimation in all weather condition is feasible by using microwave techniques that include microwave radiometry and GPS [*Cadeddu et al.*, 2013; *Wang and Zhang*, 2007]. The satellite-based microwave radiometric observations of PWV are, however, limited to the oceanic region owing to the higher land surface emissivity [*Pringent et al.*, 1997].

The application of GPS water vapor measurement with high temporal resolution in all-weather condition has been demonstrated [*Bevis et al.*, 1992] and is well established [*Duan et al.*, 1996; *Rocken et al.*, 1993]. The advantage of GPS-based water vapor measurement is that it does not require periodic calibration, besides being a low-cost, all-weather (including precipitation) technique [*Ware et al.*, 2000].

Ground-based passive microwave radiometers have been used experimentally in the past for measuring the PWV. *Guiraud et al.* [1979] demonstrated the capability of microwave radiometers to measure PWV with accuracies greater than those estimated from radiosondes. *Rogers and Schwartz* [1991] studied the mesoscale fluctuations in columnar water vapor from radiometric measurements. Mesoscale characterization of PWV and temperature were carried out over a tropical region using microwave radiometric observation during the Tropical Cyclone Experiment, 1990, on the island of Saipan by *Han et al.* [1994]. *Iassamen et al.* [2009] analyzed the distribution of water vapor under clear and cloudy conditions from microwave radiometric observation in the lower troposphere over different sites located in France. Over the equatorial region, the potential of microwave radiometer to monitor the genesis and evolution of a local convective event that lead to waterspout has been demonstrated [*Raju et al.*, 2013].

PWV is an important parameter that is closely linked to precipitation and can be used in numerical weather models. With a view to better characterize this atmospheric constituent in terms of its variability, several studies have been carried out. Interannual variability in tropospheric water vapor was examined over regions including Texas, Montana, using radiosonde data during 1958–1980 [*Angell et al.*, 1984]. *Hensc et al.* [1988] reported an upward PWV trend over the western Pacific from 1965 to 1986. Annual cycles of tropospheric water vapor using radiosonde data were reported for 56 different locations [*Gaffen et al.*, 1992]. Multiscale analysis of PWV over Africa using GPS and European Centre for Medium-Range Weather Forecasts data showed significant PWV variability over a broad range of time scales [*Bock et al.*, 2007]. All these studies are relevant to respective locations and have demonstrated their greater impact on weather and climate systems of those locations and regions.

A hyperspectral microwave radiometer profiler (MRP) (of Radiometrics model MP-3000A) has been operated continuously at TVM since April 2010, and the data for the period of 2010–2013, which includes four Asian summer monsoon (ASM) seasons (months from June to September every year), have been analyzed. The results are presented and discussed in this paper. Section 2 details the system description and the methodology used to estimate PWV from MRP and GPS data. Section 3 presents validation and intercomparison of PWV from MRP and GPS, while the rest of the sections deal with the temporal and vertical variability of water vapor and different factors responsible for these variations.

1.1. Site Description

Thiruvananthapuram (also known as Trivandrum, TVM) located at 8.5°N, 76.9°E is an equatorial coastal station which experiences tropical coastal climate with moderate temperature influenced by the Arabian Sea. Over this site, during premonsoon months (March, April, and May), severe convection tends to maximize in the late afternoon, in response to the enhanced thermodynamic instability associated with diurnal heating, resulting in summer showers and thunderstorms.

The southwest Indian peninsular region is the gateway of Indian summer monsoon. TVM experiences the onset of monsoon by the first week of June. During the southwest monsoon period (June to September), there is significant loading of water vapor, carried by southwest oceanic wind. The loading of water vapor usually begins in April (as the synoptic winds start shifting from offshore to onshore) and establishes as northwesterlies by the end of May, leading to the onset of monsoon under favorable atmospheric conditions. A strong westerly low-level jet (LLJ) stream over peninsular India during summer monsoon accounts for the transport of humid air in the lower troposphere [*Joseph and Raman*, 1966]. This westerly monsoon current gets stronger at 850 hPa typically in the month of July. These westerlies become weak and easterlies set in from October onwards. This sets the northeast monsoon, which lasts for 2 months,

October and November. The southwest summer monsoon is characterized by active and break spells, modulated by pronounced intraseasonal and interannual variability. Thus, the relevance of the study on seasonal as well as interannual variability of water vapor observations over this tropical region increases as it has greater implications on the onset, modulation, and characteristics of Indian summer monsoon. The regular ascent of radiosondes by India Meteorology Department (IMD) over TVM are available only at 00:00 and 12:00 UTC, and as such, are not suitable for diurnal and short-term temporal variation studies.

2. System Description

2.1. Microwave Radiometer Profiler

The study region, radiometer installation, and its mode of operation over TVM are detailed by *Raju et al.* [2013]. Profiler details can be found in *Cimini et al.* [2011]. The radiometer sequentially observes brightness temperatures (T_B) in 21 K band (22–30 GHz) and 14 V band (51–59 GHz) frequency channels. The bandwidth for each channel is 300 MHz. The beam width is 5–6° at 22–30.0 GHz and 2–3° at 51–59 GHz. It also includes meteorological sensors for the measurement of surface temperature, pressure, and humidity. A zenith-looking infrared (IR) radiometer and a rain detector are also attached to the radiometer for estimating cloud base height and precipitation time, respectively. The 22–30 GHz channels are calibrated to 0.3 K root-mean-square (RMS) by automated tipping procedures, and 51–59 GHz channels are calibrated to 0.5 K RMS with liquid nitrogen target [*Han and Westwater*, 2000]. The tipping calibration accounts for the different antenna beam width for the operating channels. Corrections for radiometer antenna beam width, radiometer pointing error, mean radiating temperature error, and horizontal inhomogeneity in the atmosphere on the tipping calibration for ground-based microwave radiometers are included. These corrections have been found to largely reduce or avoid calibration uncertainties and have been used with the present system.

2.1.1. Water Vapor Retrieval From MRP

MRP measurements of the atmospheric thermal emissions at 22–30 GHz channels are used to retrieve PWV and water vapor profiles. A neural network [*Solheim et al.*, 1998] trained with historical data from TVM radiosondes is used to retrieve temperature, humidity, and liquid profiles from multichannel T_B, surface meteorological parameters, and zenith infrared measurements. The profiles extend to 10 km height with 50 m steps up to 500 m, 100 m steps to 2 km, and 250 m steps to 10 km. Radiometer temperature and humidity profile comparisons with collocated radiosondes show radiosonde-equivalent observation accuracy [*Cimini et al.*, 2011; *Gueldner and Spankuch*, 2001; *Knupp et al.*, 2009]. Besides profiles, PWV and integrated liquid water are also retrieved. Microwave radiometers are widely used to calibrate radiosonde PWV measurements [*Cadeddu et al.*, 2013]. Heavy rain degrades radiometer retrieval accuracy. However, this effect was minimized using off-zenith (15° elevation) observations [*Xu et al.*, 2014].

2.2. Global Positioning System

A triple-frequency GPS receiver, Leica GRX1200/GNSS, has been installed at the radiometer site and operational since May 2010, and it receives radio signal at L1 (1.57 GHz), L2 (1.227 GHz), and L5 (1.110 GHz) frequencies. A meteorological sensor (MET3) has been also installed close to the GPS antenna location for temperature, relative humidity, and pressure measurements. As the microwave GPS signal propagates through the atmosphere, it gets refracted as well as retarded due to variability in the refractive index of the atmosphere. The ionosphere is a frequency-dependent dispersive medium, allowing dual- (or multi) frequency observations to be used to estimate the delay due to ionosphere with fairly good accuracy. The net delay term left out would be the tropospheric delay and the tropospheric delay in the zenith direction, called zenith tropospheric delay (ZTD), which has two parts: one part is governed by the nonpolar gases (hydrostatic), usually referred to as zenith hydrostatic dry delay (ZHD), and the other component delay contributed by polar molecules (nonhydrostatic) like water vapor which is referred to as the zenith wet delay (ZWD). While the hydrostatic (dry) component constitutes about 90% of the total delay, the nonhydrostatic (wet) part constitutes the remaining 10% [*Bevis et al.*, 1992].

If the position of the receiver is accurately known, the ionospheric delay is estimated with a fairly good accuracy using multifrequency measurements, then it will be possible to estimate the integrated columnar water vapor overlying the receiver from the GPS signals, making use of the data on surface pressure and temperature at the same location [*Bevis et al.*, 1994; *Duan et al.*, 1996; *Rocken et al.*, 1993, 1995].

Askne and Nordius [1987] attempted to relate the PWV and ZWD through a linear relation given as

$$PWV = \Pi \times ZWD \qquad (1)$$

Π is the proportionality coefficient related to the weighted mean temperature T_m [*Askne and Nordius*, 1987; *Bevis et al.*, 1992; *Liou et al.*, 2001] as

$$\Pi = \frac{10^8}{\rho_l R_v \left[\left(\frac{k_3}{T_m} \right) + k_2' \right]} \qquad (2)$$

where ρ_l is the liquid water density (kg m^{-3}) and R_v are the gas constant for water vapor (461 J kg^{-1} K^{-1}) and hydrostatic refractivity constants ($k_2 = 64.79$ K hPa^{-1} and $k_3 = 3.776 \times 10^5$ K^2 hPa^{-1}). The variation of the proportionality coefficient (Π) with temperature is taken into account through T_m (in kelvin) defined [*Bevis et al.*, 1994] as

$$T_m = \frac{\int \left(\frac{e(z)}{T(z)} \right) dz}{\int \left(\frac{e(z)}{T^2(z)} \right) dz} \qquad (3)$$

where $e(z)$ is the water vapor partial pressure (hPa) at z height levels.

The previous studies relating PWV and ZWD over other two tropical stations in Indian peninsular inland regions like Bangalore and Hyderabad [*Raju et al.*, 2007] were obtained through regression analysis, yielding a correlation coefficient of 0.999 are

$$PWV(mm) = (0.153 \pm 0.00016) \times ZWD \qquad (4)$$

$$PWV(mm) = (0.156 \pm 0.00014) \times ZWD \qquad (5)$$

The similar empirical relation for TVM station is discussed in section 3.1.1.

2.3. Radiosonde Observations

Radiosonde observation from the IMD TVM station (8.48°N, 76.95°N; located at an aerial distance of ~3 km from MRP site) has been used for the analysis. The radiosonde used at this station is Mark III, developed by IMD [*Jain et al.*, 2006] with uncertainty of ~60 m in height and 0.4 K for temperature at ~100 hPa pressure level. The precision determined for IMD radiosondes is ~0.66 K, and an intercomparison of this radiosonde with World Meteorological Organization certified U.S. sondes reported a mean difference as well as the standard deviation <1 K [*Sunilkumar et al.*, 2013]. The PWV is obtained by integrating water vapor density profile estimated from radiosonde measured temperature and dew point temperature profiles [*Raju et al.*, 2007]. The regular radiosonde soundings were available at 00:00 and 12:00 UTC. The radiosonde profile with ascents above 12 km altitude under clear-sky condition during 2010 are considered for this study. Several types of systematic errors in global radiosonde PWV data have been reported by *Wang and Zhang* [2007] based on the comparison with GPS PWV data.

3. Results

3.1. Validation of MRP-Derived PWV With Collocated GPS Measurements

Water vapor estimation from MRP and GPS observations are based on two different physical processes for microwave propagation through the atmospheric medium. Attenuation and thermal emission are the basic physical processes involved in the MRP-based PWV estimation, while in case of GPS, PWV quantification is mainly through the refraction and retardation processes due to the polar nature of water vapor molecules. The frequency domain used in GPS measurements at L band is not affected by the clouds and rain. On the other hand, the radiometric observations at Ka and V bands have significant effect by precipitation due to the thermal emission from the water droplets, settled on the top of the radome, when radiometer antenna is pointing at zenith direction. Thus, heavy rain degrades radiometer retrieval accuracy. As mentioned before, this effect has been minimized using off-zenith (at 15° elevation) observation and retrieval methods [*Xu et al.*, 2014].
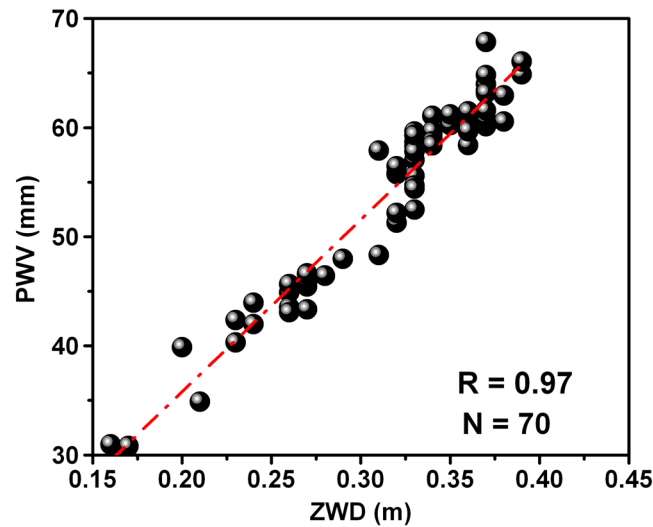
Figure 1. Scatterplot showing dependence of PWV from radiosonde and ZWD from GPS.

As such, it is essential to intercompare the PWV estimates from these two techniques especially over the tropical atmospheric condition during Indian summer monsoon period when there is large loading of water vapor.

3.1.1. Developing Empirical Model for PWV Estimation From Ground-Based GPS Receiver Measurements

The GPS data were processed using GAMIT software package (developed by Massachusetts Institute of Technology and Scripps Institute of Oceanography) to estimate three-dimensional relative positions of ground points and satellite orbits from GPS data. The GAMIT uses the GPS data in the receiver-independent exchange format collected at our station along with eight other International GPS Service stations, which are chosen based on a thorough optimization study *Tregoning et al.* [1998]. The GAMIT estimates the propagation delay mapped to zenith direction [*Niell*, 1996]. ZHD is then estimated by substituting the pressure values measured at the GPS antenna position and using station-based models developed for TVM [*Korak et al.*, 2007] which employs the atmospheric pressure (P_s) measured at the antenna position. ZHD component is then subtracted from ZTD to estimate ZWD.

As ZWD depends primarily on the atmospheric water vapor content, this parameter can be related with PWV. The quantity of water vapor in the atmosphere is temperature dependent, and both these parameters vary with altitude also. In order to account for the effect of vertical structure of atmospheric temperature in the estimation of PWV, a parameter called the weighted mean temperature (T_m), which is the water vapor weighted vertically averaged temperature, has been used. An empirical relation between T_m and surface temperature (T_s) has been established by *Davis et al.* [1985].

But in tropics where the correlation between T_m and T_s decreases significantly owing to the fact that the range of T_s variations is rather small. In case of TVM, with its proximity to the equator, the seasonal and diurnal variations of surface temperatures are very small <10 K. Hence, a simple linear regression relating PWV and ZWD is appropriate as reported in *Raju et al.* [2007]. A station-based linear regression model relating PWV from ZWD has been generated, which does not require T_s measurements as well. The regression analysis, as shown in Figure 1, the PWV values used are obtained from about 70 good radiosonde profiles that had ascends above 12 km altitude under clear-sky condition.

$$\text{PWV (mm)} = (0.157 \pm 0.0047) \times \text{ZWD} \qquad (6)$$

This empirical relation yields a correlation coefficient of 0.97 and has been used for estimating PWV from the GPS-derived ZWD. The accuracy of this model is examined by comparing the retrieved PWV from radiosonde, and it is found to be ~2.03 mm.

3.1.2. Intercomparison of PWV Obtained From MRP and GPS Data

The regression analysis between PWV derived from MRP (PWV$_{MRP}$), measurements at every 1 min interval are averaged for 30 min and PWV derived from GPS data (PWV$_{GPS}$), during May 2010 to December 2010, is shown in Figure 2 (left), which shows a good correlation of 0.98 and RMS difference of 1.6 mm. The GPS measurements underestimate the PWV by 4 to 5%, mostly during highly humid condition (PWV > 60 mm). *Pérez-Ramírez et al.* [2014] also have reported a small overestimation of PWV by microwave radiometer. Therefore, further studies are required to understand the discrepancies of PWV measurements under highly humid conditions. The percentage distribution of difference between the PWV values from two instruments, shown in Figure 2 (right), shows that it follows Gaussian distribution with more than 70%
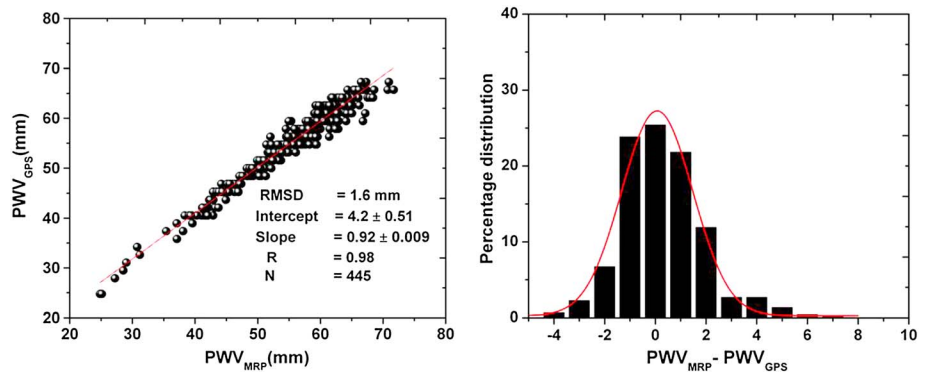
Figure 2. (left) Scatterplot showing correlation between PWV from GPS (PWV_{GPS}) and that from MRP (PWV_{MRP}). (right) Histogram of the difference between PWV_{MRP} and PWV_{GPS}.

differences lying within ±1 mm and 20% lying within ±1 mm to ±2 mm, thereby indicating an excellent agreement except during high humid condition where it shows small positive skewness.

A one-to-one comparison of PWV_{MRP} and PWV_{GPS} for 8 month period from May 2010 to December 2010 has been made. Figure 3 (top) shows the one-to-one comparison between PWV_{MRP} and PWV_{GPS} during the period (day of year (DOY) 121 to 365) when GPS measurements are available. Figure 3 (bottom) shows the daily accumulated rainfall collected from the collocated rain gauge and disdrometer measurements.

Figure 3 shows a good agreement between the PWV_{MRP} and PWV_{GPS} during the period which includes both active and break periods of monsoon with respect to the station. Good agreement observed between the two PWV values during the heavily rainy days such as 280, 325, and 342 Julian days (DOY) besides the good agreement observed for nonrainy days. This further implies the consistency and potential of MRP measurements over the equatorial coastal station under heavy water vapor loading condition during the monsoon period.

The PWV in the premonsoon month, May, shows significantly large variability between 45 and 70 mm, which is attributed to frequent local convective events and the low depressions forming after mid-May (DOY 138–149). From June to September (DOY 152–274), the monsoon prevails over the region and is influenced by the overcast monsoon clouds. The active spells are characterized by well-distributed and continuous rainfall over
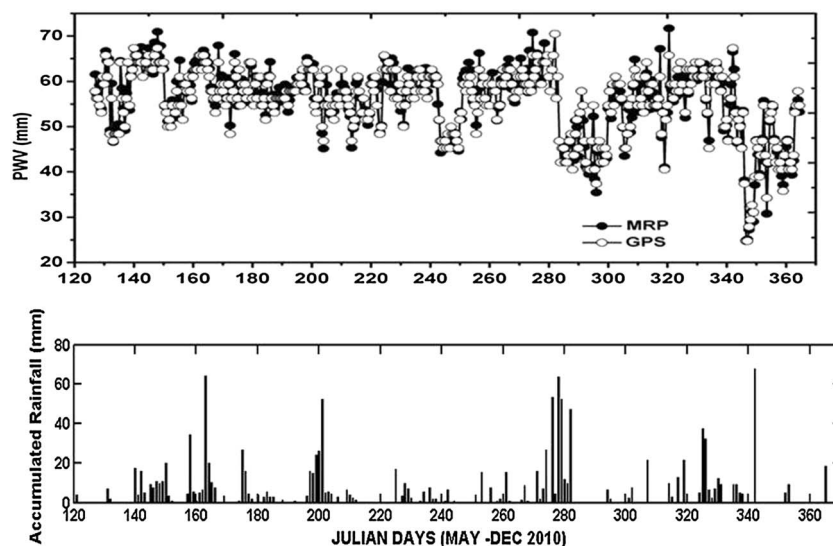

Figure 3. (top) Comparison of PWV_{GPS} and PWV_{MRP} from May to December 2010. (bottom) Accumulated rainfall measured using disdrometer and rain gauge at MRP site for the same period.
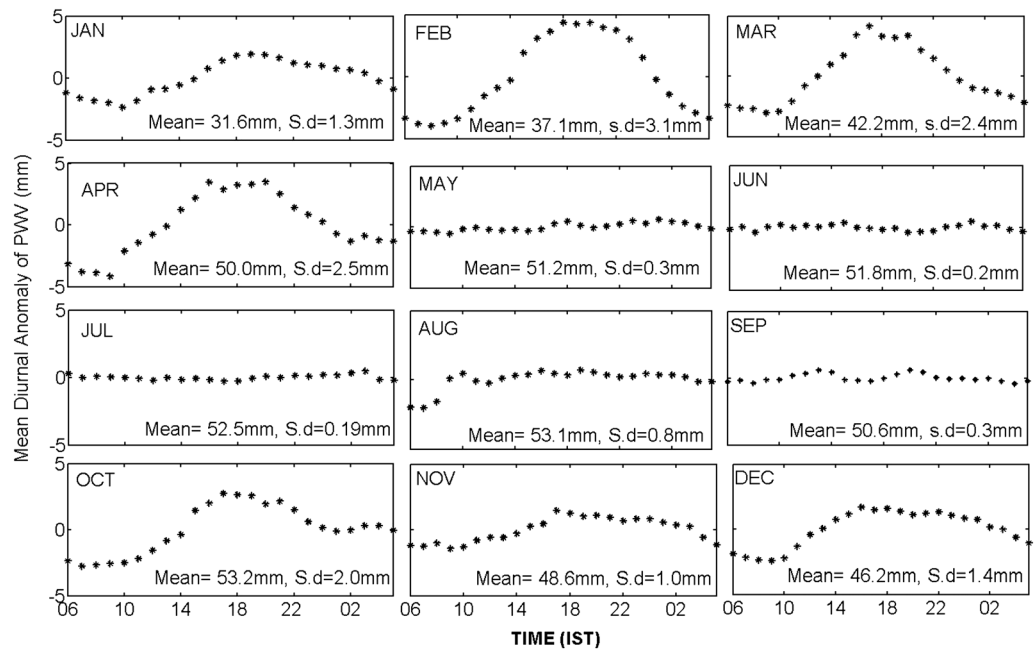
Figure 4. Mean diurnal anomaly of PWV with monthly mean (mm) and standard deviation (mm) shown on the top of each plot.

the station location, whereas break spells are the periods when this large-scale rainfall is interrupted for several days in the peak monsoon months of July and August [*Malurkar*, 1950]. The southwest monsoon period (June to September) has active and break spells as seen in Figure 3, and during the retreating phase of monsoon (northeast monsoon), the year 2010 experienced good rainfall as seen in the months of October–November (~161 mm). The heavy rain event occurred on 8 December, resulted in a rainfall of ~70 mm/h at 03:00 LT, and soon after the event, the atmosphere become dry with low PWV value of 35 mm associated with lifting up of the cloud base height above 5 km. Both the techniques were able to pick these variabilities in water vapor as observed in Figure 3.

These analyses imply that the microwave radiometric measurements of PWV over the tropical station are consistent throughout the measurement period, and hence, these measurements have been used to study the seasonal and interannual variability of PWV and the effect of monsoon on PWV distribution.

3.2. Diurnal Cycle in PWV and Its Seasonal Variation

The continental dry wind prevailing over the station during winter period (December to February) causes low atmospheric humidity. Being a tropical coastal station, the water vapor variability in winter season at TVM is greatly influenced by the diurnal heating of the land surface as well as thermally induced local circulations such as the land and sea breeze circulations. This would result in a diurnal anomaly in PWV which has been examined by studying the continuous MRP measurements of PWV for 3 years (2011–2013). The diurnal anomaly of PWV is obtained by removing the daily mean from hourly observations and thus arriving at the monthly mean diurnal anomaly. This equivalent day analysis has been carried out to bring out the deviation of PWV on daily basis, and then the mean for each month is generated from the continuous daily MRP observations. The monthly mean diurnal anomaly of PWV with monthly mean and the mean standard deviation of day-to-day variation of PWV diurnal anomalies (in millimeter) are indicated on the top of each plot of Figure 4. The winter period and premonsoon period (March and April) show significant diurnal variability in PWV. A distinct diurnal variation in PWV is observed with the minimum reaching between 06:00 and 09:00 IST (Indian standard time in hour) in the morning and gradually increasing during the daytime reaching its maximum in the evening between 16:00 and 19:00 IST. The amplitude of the peak is highest in February, and it reaches to >4 mm.
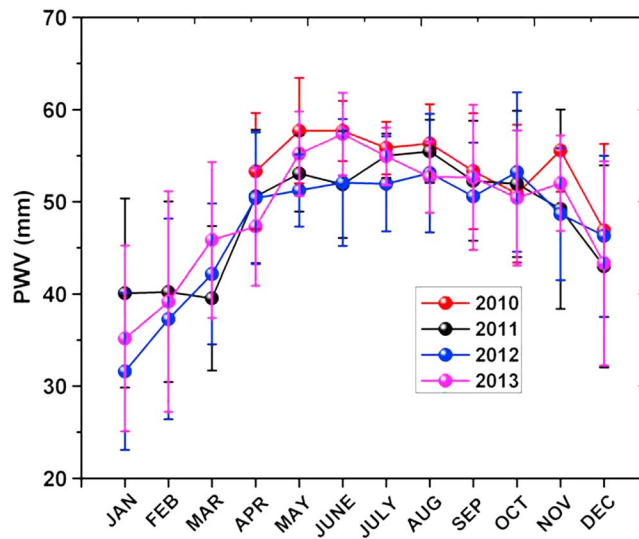
Figure 5. Interannual variability of PWV with standard deviation for 4 years (April 2010–December 2013).

TVM being a coastal station, the influence of sea and land breezes also play a significant role in the transport of water vapor during winter and premonsoon periods. During daytime, there is a dry anomaly observed due to the process of surface evaporation, resulted from the strong summer equatorial heating, besides the transpiration which accumulates the water vapor and latent heat in lower atmosphere level. This forms a conducive state for the genesis of convection. The station experiences the occurrence of frequent local convective systems during the premonsoon summer period. These systems can have genesis over land as well as over sea usually in the late afternoon and maximize in the late evening hours [*Raju et al.*, 2013], in response to the enhanced thermodynamic instability associated with strong diurnal heating. Soon after the convection breaks out, the wet anomalies are observed during late nighttime. Once humidity-bearing monsoon sets over the station, the diurnal variability has been vanished, owing to the advection of water vapor due to strong low-level jet which sets on after mid-May and persists for southwest monsoon period. The persistence of overcast, continuous rain during the active phase of monsoon over this station also results in lack of diurnal variability of PWV during monsoon months.

3.3. Seasonal and Interannual Variability of PWV

The interannual variability of PWV in terms of monthly mean, with the standard deviations, for the 4 years from April 2010 to December 2013 is shown in Figure 5. The standard deviation shown as vertical lines indicates the variability of PWV in each month. PWV is large during May to November for all the years. During December to March, PWV ranges between 30 and 45 mm with large standard deviations (10 to 12 mm), which indicates that water vapor is highly variable during this period. During the southwest Indian monsoon (SWM) period (June–September) and during the transition of SWM to northeast monsoon (NEM) period (usually in October), the range of PWV is between 50 and 60 mm with least standard deviation (2 to 5 mm) indicating very less variability in PWV during the monsoon period. The interannual variability is also very low in PWV during this period over this station. During winter and premonsoon periods, the moisture incursion is primarily associated with the sporadic weather events. Moreover, during winter, the wind direction is highly variable and weak which can occur from the ocean or from the land. During premonsoon months, the wind gets slightly strengthened, but it is still variable. During SWM period, the wind direction is highly stable and persistently occurs from the Indian Ocean, although wind speed can be highly variable. Due to the proximity to the ocean, although the wind speed is variable, the persistent wind from the ocean brings moisture to this coastal station, which results in less variability of PWV during monsoon period.

The monthly accumulated rainfall during the monsoon periods show significant interannual variability in rainfall with maximum in 2013 as shown in Figure 6. The year 2012 is the year when this station experienced least rain. The analysis shows interannual variability in precipitation rate; however, there is no significant variability observed in PWV, which demands the further investigation on the vertical structure of water vapor as it describes the transport of water vapor to different altitude levels due to the combined effect of advection and convection particularly during monsoon period.

3.4. Vertical Distribution of Specific Humidity

The vertical variability of water vapor and its significance during the onset, active, and break spells of monsoon are examined for the consecutive 4 years (2010–2013) by analyzing the variation of the specific
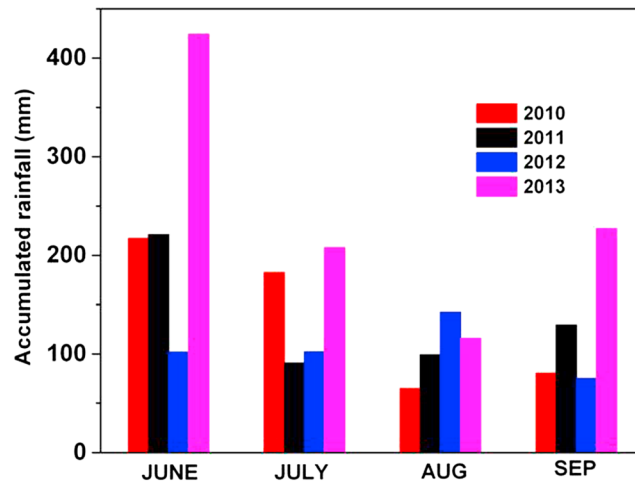
Figure 6. Interannual variability of accumulated rainfall from collocated rain gauge and disdrometer measurements for the monsoon period for 4 years (2010–2013).

humidity (the ratio of the mass of water vapor in a given volume to the mass of air in the given volume, at different altitude). Due to the proximity to the equator and to the sea coast, the specific humidity in the 0–2 km altitude layer, always, prevails higher than ~18 g/kg over the station. The maximum variability of specific humidity observed in this layer is from 12 to 18 g/kg during extreme dry conditions. The variability in water vapor is mainly observed in the altitude level of 2–6 km, and its relation with the active and break phases of the monsoon spell are examined.

Figures 7–9 show the distribution of specific humidity at 2–8 km altitude level, respectively, during the premonsoon months (April and May), during the monsoon period (June to September), and during postmonsoon period (October and November) for 4 years. Figure 7 shows that there is a positive gradient in specific humidity with days as well as with altitude, which is the indication of the continuously increasing water vapor
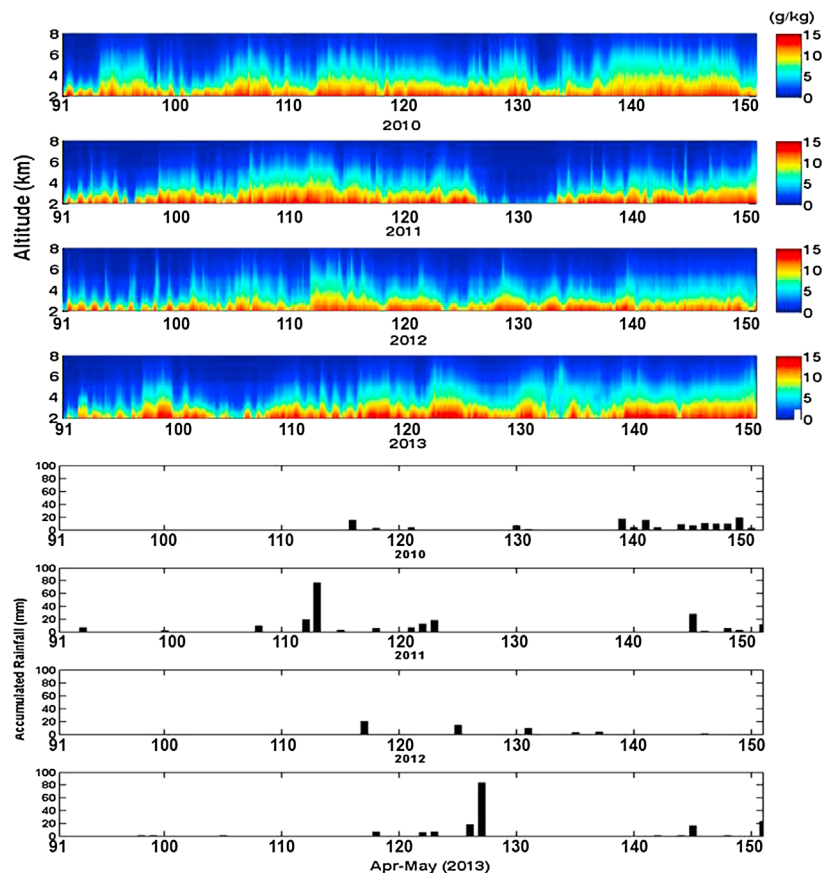

Figure 7. Vertical distribution of specific humidity in the 2–8 km altitude range and accumulated rainfall during 1 April to 31 May for 4 years (2010–2013).
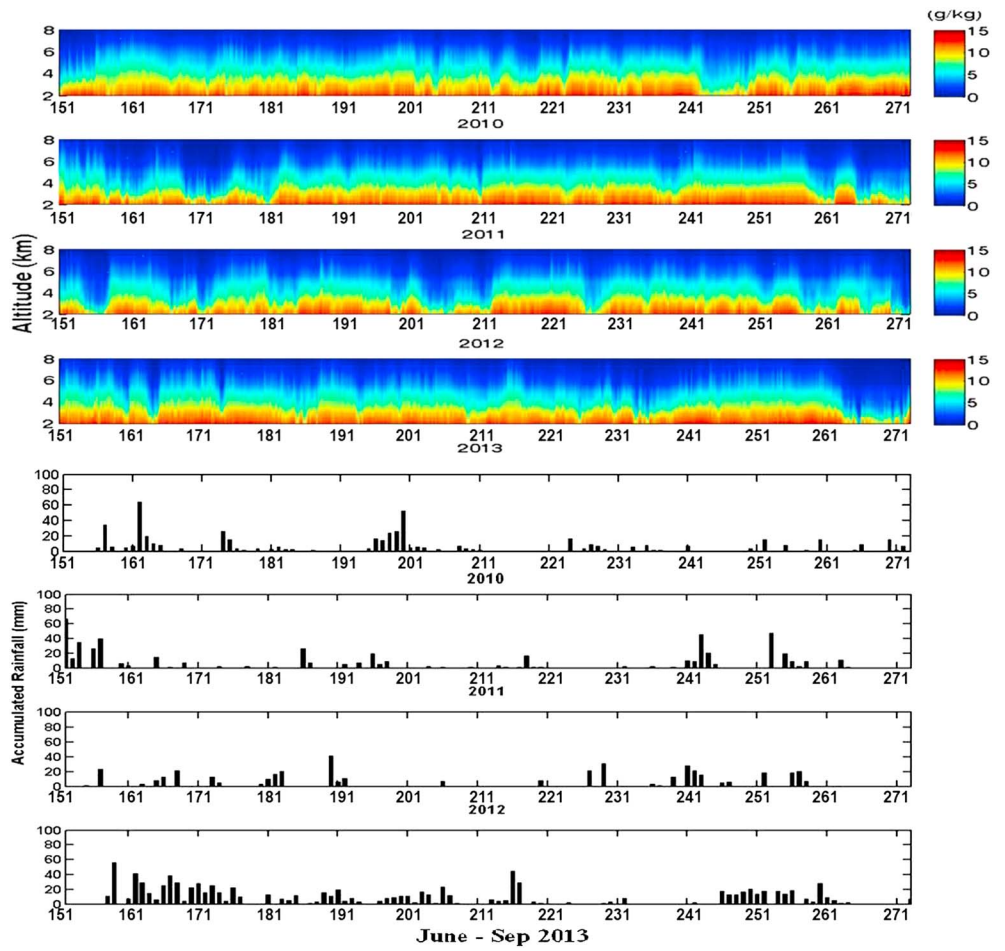
Figure 8. Vertical distribution of specific humidity in the 2–8 km altitude range during June–September (monsoon period) from 2010 to 2013 with accumulated rainfall shown in lower plots.
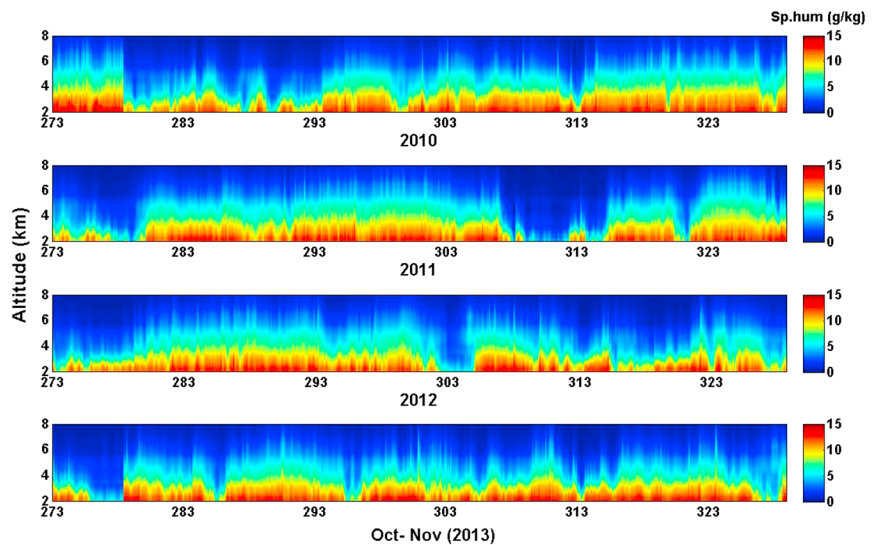

Figure 9. Vertical distribution of specific humidity in the 2–8 km altitude range during October to November (postmonsoon period) from 2010 to 2013.

loading in the upper levels during the premonsoon months (April and May). In the year 2010, the continuous building up of water vapor began from mid-May and humidity reaching ~5 g/kg at 6 km altitude level and resulted in moderate rain with more number of active spells. The year 2012 experienced only weak tropical convections, the building up of humidity was slow and less intense limiting the higher moisture level to ~4 km altitude, whereas in 2013, the building up was strong and intense and humidity greater than ~5 g/kg reaching to altitude level beyond 6 km by the end of May.

The onset of monsoon is associated with the indication of monsoon rains, and it usually hits over the Kerala coast of the Indian mainland on 1 June, and this onset day usually varies from year to year with ±5 days [*Ananthakrishnan et al.*, 1967]. The variation of the vertical structure of humidity during the onset phase of the Asian summer monsoon (ASM) period is shown in Figure 8. Once the humidity value (~5g/kg) reaches in upper altitude level, above 5 km as observed, the onset of monsoon is occurring, and throughout the active period higher, the humidity value is maintained consistently in that altitude region.

In the year 2010, the humidity building up that started from mid-May due to the formation of depression over Arabian Sea resulted in continuous rain for 10 days, resulting in a "bogus" onset of monsoon as declared by the IMD on 31 May. This was followed by the weakening of depression, and the humidity at upper level decreased. It took almost 1 week for humidity to build up in the upper level, which lead to the active spell again. After the first week of June, the active spells are dominant, and the upper level humidity drastically decreased from 30 August to 9 September as seen in Figure 8, which was the break period over this station. In 2011, the onset occurred on 29 May, and after 10 days, the upper level humidity (>5 km) decreased, and again, dry condition repeated after 10 days. Such a pulsating nature in PWV is observed in the month of June. After July, the active period occurred with two significant break periods on 12 July and 24 September. In 2012, the building up of humidity was slow as discussed earlier, and the onset was also delayed by 5 days. Soon after the onset, a break spell occurred. The year 2012 experienced more number of break spells with longer period than the active spells, and duration of active spells were also shorter. Hence, during this period, large variability in specific humidity at altitude levels above 2 km is observed, and no such consistent water vapor building up is taking place, which might be resulting in rainfall deficit year [*Simon and Joshi*, 1994].

The humidity distribution in 2 to 6 km altitude range is in accordance with the active and break phases of the monsoon period. Figure 8 shows that the vertical variability of water vapor during the monsoon period of the year 2010 varies in the range of 8–11 g/kg, while during the break period, it fell to low value of ~6 g/kg as seen in the beginning of September. In 2011, during active spell, the humidity varies in the range of ~7 to ~10 g/kg and fell to a low value of ~5 g/kg during the time of break periods. In 2012, specific humidity shows large variability unlike that in the previous years, which makes it difficult to differentiate break and active spells. The humidity values reached even $< \sim 4$ g/kg at this altitude level, indicating the prevalence of dry atmosphere even during the monsoon period. In 2013, no typical break period is observed during the season, and rainfall pattern shows break-like condition in the end of August, which could be due to the weakening of monsoon circulation.

Usually, the SWM weakens by the middle and end of September, but in 2010 after the break period, the system get strengthened and resulted in heavy rain until first week of October, which is due to the formation of depressions and resulted in the delayed withdrawal of SWM in that year as shown in Figure 9 [*Tyagi et al.*, 2010]. Figure 9 shows that in the year 2011, the NEM got activated by mid-October, and in November, break period of 5 days occurred associated with the high-pressure systems over Arabian Sea, similar to that observed in the month of May, showing that these are the months when these kinds of systems are generally occurring over this region. By December, the availability of humidity started decreasing in upper altitude levels. This kind of analysis helps to understand the humidity distribution at different altitude levels and its impact on monsoon spell as seen that the vertical gradient of humidity in 2 to 6 km altitude layer is associated with the strength of the monsoon.

4. Discussion

Besides the general multiscale features discussed in the above sections, the continuous microwave radiometric observations are also useful to study the drastic variation of the atmospheric system for the
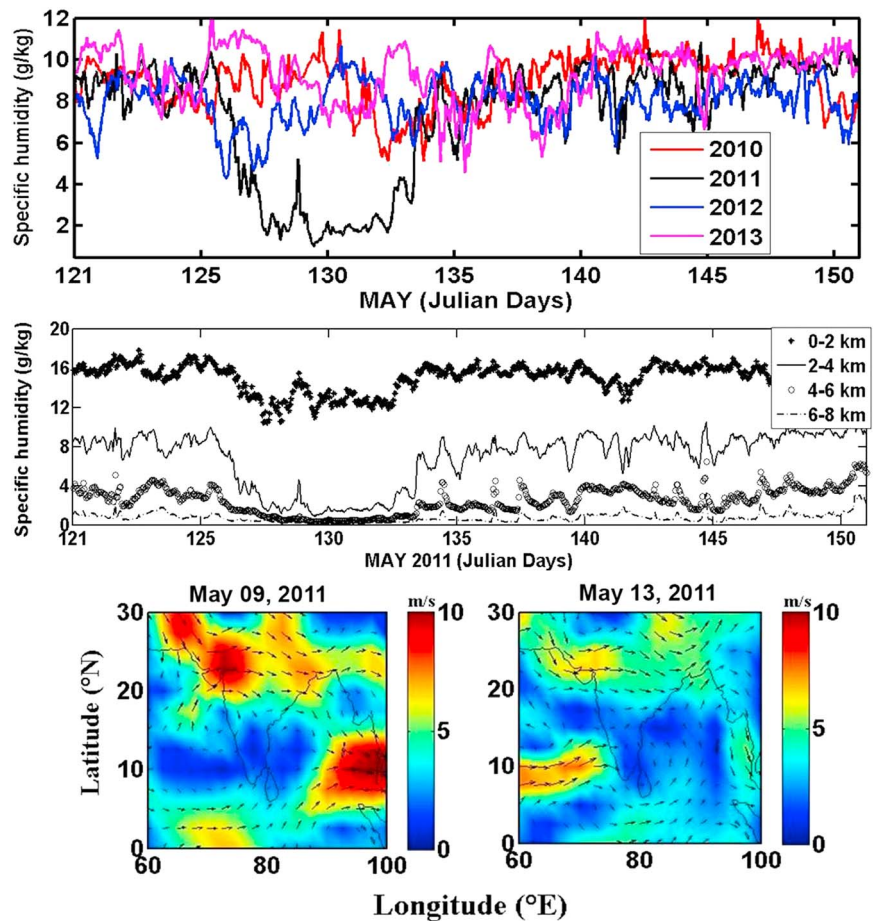
Figure 10. (top) The temporal variation of specific humidity in May during 4 years 2010–2013 at 2–4 km altitude level. (middle) The temporal variation of humidity at four different altitude levels (0–2, 2–4, 4–6, and 6–8 km) for the year 2011. (bottom) The background wind condition at 850 hPa (NCEP/NCAR data) on 9 May (during the high-pressure system developed over Arabian Sea) and after the event on 13 May 2011.

short time period. The detailed investigation on such atmospheric phenomenon and its link with the monsoon is given in the following section.

The humidity variation at 2 km altitude during May 2010, 2011, 2012 and 2013 is shown in Figure 10 (top). In 2011, from 7 to 11 May, the specific humidity fell to <2g/kg from the preexisting value of ~8 g/kg, and hence, the region experienced an unusual extremely dry atmospheric condition as shown in Figure 10 (top). The specific humidity distribution in different altitude levels are shown in the Figure 10 (middle), and it also shows that the humidity drastically reduced in the altitude level of 2 to 4 km and least variation observed in the 6 to 8 km level. The cloud base height, observed by the IR radiometer attached with MRP, was also higher (>7 km) during this period, showing clear-sky conditions, devoid of any clouds. The background winds, estimated from the National Centers for Environmental Prediction (NCEP)/National Center for Atmospheric Research (NCAR) reanalysis data (2.5° × 2.5°) and shown in Figure 10 (bottom), indicated the development of a high-pressure system over the Arabian Sea. The air mass back trajectory analyses also indicated that during this period, dry air mass was being advected from Indian mainland and from west of Asia at the 3000 m altitude level which descended at the location resulting in such dry condition over this coastal station. The large humidity building up started soon after this dry stage as southwest winds strengthen and transport humidity from sea to land.

In 2013, the region experienced good monsoon (prolonged active spells occurring during monsoon period whereas during poor monsoon period, long dry spells are occurring) [*Rajeevan et al.*, 2010] with onset on 1 June. The PWV from MRP observations during monsoon period also show high value during this year as
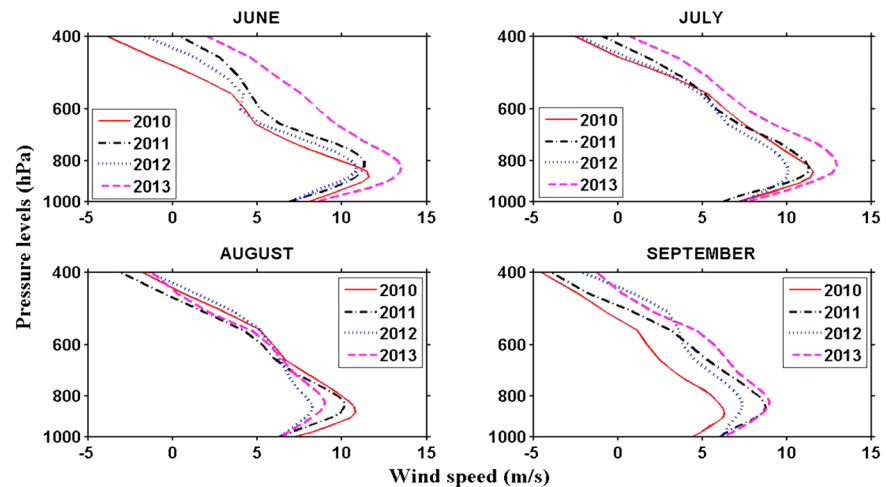
Figure 11. Vertical profile of wind (MERRA data) for June, July, August, and September (monsoon period) from 2010 to 2013.

seen in Figure 5. Figure 6 shows that heavy rainfall is obtained during the months of June, July, and September in this year. Figure 7 shows that by the end of May, there is a strong building up of humidity taking place in the upper altitude levels reaching to >6 km. Figure 8 shows that there is large humidity available in the upper altitude level resulting in continuous active spells with very less break spells which might resulted in good monsoon over this site. In bringing the monsoonal rains over India, the cross equatorial flow of moisture as well as the evaporation over the north Indian Ocean and adjoining seas plays an equally important role [*Pisharoty*, 1965; *Saha and Bavadekar*, 1973]. An analysis on the vertical structure of zonal wind component, aimed to examine the role of wind on water vapor variation, has been carried out for the monsoon period (June to September), using Modern-Era Retrospective Analysis for Research and Applications (MERRA) data (0.5°×0.67°) for the 3 year period from 2010 to 2013, and results are shown in Figure 11. The core of the LLJ lies in the 850 hPa, and its influence extend up to 6 km [*Joseph and Sijikumar*, 2004]. The figure shows that the flow of moisture is stronger during the year 2013 compared to last 2 years and least in the year 2012. It shows that LLJ was strong during 2013 especially in the months of June and July, which might resulted in the large transport of humid air and resulted in good monsoon, whereas the weak LLJ during 2012 led to rainfall deficit year over this region. *Joseph and Sijikumar* [2004] reported that the strength of LLJ is an important factor in determining the active and break spells during monsoon period. The influence of LLJ on the active and break spells of monsoon and effect of intraseasonal oscillations on the humidity variation and dynamics of monsoon will be further investigated in detail for this station.

5. Conclusion

The study of water vapor variability over the tropical station is important to understand the influence of water vapor on small-scale weather phenomena like convection to complex and organized phenomena like monsoon. This paper presented the diurnal, seasonal, interannual, as well as vertical variability of water vapor from multiyear microwave radiometric observations over an Indian tropical station, TVM. The potential, accuracy, and consistency of microwave radiometric measurements of water vapor over equatorial coastal condition including the monsoon period have been established by comparing the concurrent and collocated measurements by GPS and MRP.

A station-based linear regression model for the tropical atmosphere at TVM has been developed to derive PWV from GPS wet tropospheric delay component. The comparison of PWV estimated from GPS data and that from MRP in all seasons including monsoon period yielded correlation coefficient 0.98 and RMS difference of 1.6 mm; this proves the reliability of PWV from MRP observations. During premonsoon and winter periods, the diurnal variability in water vapor exists which vanishes during the monsoon period. No significant interannual variability in PWV is observed as seen in the rainfall pattern. The vertical distribution

of specific humidity in the altitude levels 2–6 km exhibits significant interannual variability and is related to the monsoon activities such as the active and break spells.

Prior to the onset of monsoon, the specific humidity ~7 g/kg reaches to above 5 km altitude level and is consistently maintained there during active spells. However, when there is no such consistent water vapor buildup, large variability in humidity occurs in the altitude level above 2 km over this station resulting in a rainfall deficit year. The vertical wind patterns for monsoon period shows that the strength of LLJ governs the transport of humid air in the lower-altitude level and hence determines the humidity availability over this site. The different factors responsible for diurnal variability and transport of water vapor, monsoon dynamics, and effect of LLJ on active spells and influence of intraseasonal oscillations on the precipitation have to be further investigated.

References

Ananthakrishnan, R., U. R. Acharya, and A. R. Ramakrishnan (1967), On the criteria of declaring the onset of the south west monsoon over Kerala. IMD, Forecasting manual no iv-18.i, IMD, New Delhi.

Angell, J., W. P. Elliot, and M. E. Smith (1984), Tropospheric humidity variation at Brownsville, Texas and Great Falls, Montana, 1958-80, *J. Clim. Appl. Meteorol.*, *9*, 1286–1295.

Askne, J., and H. Nordius (1987), Estimation of tropospheric delay for microwave from surface weather data, *Radio Sci.*, *22*, 379–386, doi:10.1029/RS022i003p00379.

Bevis, M., S. Businger, T. A. Herring, C. Rocken, R. Anthes, and R. Ware (1992), GPS meteorology: Remote sensing of atmospheric water vapor using Global Positioning System, *J. Geophys. Res.*, *97*, 15,787–15,801, doi:10.1029/92JD01517.

Bevis, M., S. Businger, S. Chiswell, T. A. Herring, R. Anthes, C. Rocken, and R. Ware (1994), GPS meteorology: Mapping zenith wet delays onto precipitable water, *J. Appl. Meteorol.*, *33*, 379–386.

Bock, O., F. Guichard, S. Janicot, J. Lafore, M. N. Bouin, and B. Sultan (2007), Multiscale analysis of precipitable water vapor over Africa from GPS data and ECMWF analyses, *Geophys. Res. Lett.*, *34*, L09705, doi:10.1029/2006GL028039.

Cadeddu, M. P., J. C. Liljegren, and D. D. Turner (2013), The Atmospheric Radiation Measurement (ARM) program network of microwave radiometers: Instrumentation, data, and retrievals, *Atmos. Meas. Tech.*, *6*, 2359–2372.

Cimini, D., E. Campos, R. Ware, S. Albers, G. Graziano, J. Oreamuno, P. Joe, S. Koch, S. Cober, and E. Westwater (2011), Thermodynamic atmospheric profiling during the 2010 Winter Olympics using ground-based microwave radiometry, *IEEE Trans. Geosci. Remote Sens.*, *49*(12), 4959–4969.

Dai, A., and C. Deser (1999), Diurnal and semidiurnal variations in global surface wind and divergence fields, *J. Geophys. Res.*, *104*, 31,109–31,125, doi:10.1029/1999JD900927.

Dai, A., J. Wang, R. H. Ware, and T. H. Hove (2002), Diurnal variation in water vapor over North America and its sampling errors in radiosonde humidity, *J. Geophys. Res.*, *107*(D10), 4090, doi:10.1029/2001JD000642.

Davis, J. L., T. A. Herring, I. I. Sharipo, E. E. Rogers, and G. El-gered (1985), Geodesy by radio interferometry: Effects of atmospheric modelling errors on estimates of baseline length, *Radio Sci.*, *20*, 1593–1607, doi:10.1029/RS020i006p01593.

Duan, J., M. Bevis, P. Fang, Y. Bock, S. Chiswell, S. Businger, C. Rocken, F. Solheim, and T. V. Hove (1996), GPS meteorology: Direct estimation of the absolute value of precipitable water, *J. Appl. Meteorol.*, *35*, 830–838.

Gaffen, D. J., A. Robock, and W. P. Elliott (1992), Annual cycles of tropospheric water, *J. Geophys. Res.*, *7*, 2489–2502.

Gueldner, J., and D. Spankuch (2001), Remote sensing of the thermodynamic state of the atmospheric boundary layer by microwave radiometry, *J. Atmos. Oceanic Technol.*, *18*, 925–933.

Guiraud, F. O., J. Howard, and D. C. Hogg (1979), A dual-channel microwave radiometer designed for measurements of precipitable water vapor and liquid water, *IEEE Trans. Geosci. Electron.*, *17*, 129–136.

Han, Y., and E. R. Westwater (2000), Analysis and improvement of tipping calibration for ground based microwave radiometers, *IEEE Trans. Geosci. Remote Sens.*, *38*, 1260–1276.

Han, Y., J. B. Snider, E. R. Westwater, S. H. Melfi, R. A. Ferrarc, and D. W. Thomson (1994), Multichannel microwave radiometric observation at Saipan during the 1990 Tropical Cyclone Experiment, *J. Atmos. Oceanic Technol.*, *11*, 110–121.

Held, L. M., and B. J. Soden (2000), Water vapor feedback and global warming, *Annu. Rev. Energy Environ.*, *25*, 441–475.

Hensc, A., P. Krahe, and H. Flohn (1988), Recent fluctuations of tropospheric temperature and water-vapour content in the tropics, *Meteorol. Atmos. Phys.*, *38*, 215–227.

Iassamen, A., H. Sauvageot, N. Jeannin, and S. Ameur (2009), Distribution of water vapor during clear and cloudy conditions, *J. Appl. Meteorol. Climatol.*, *48*, 600–615.

Jain, A. R., S. S. Das, T. L. Mandal, and A. P. Mitra (2006), Observations of extremely low temperature over the Indian tropical region during monsoon and post monsoon months: Possible implications, *J. Geophys. Res.*, *111*, D07106, doi:10.1029/2005JD005850.

Joseph, P. V., and P. L. Raman (1966), Existence of low level westerly jet-stream over peninsular India during July, *Indian J. Meteorol. Geophys.*, *17*, 407–410.

Joseph, P. V., and S. Sijikumar (2004), Intraseasonal variability of the low-level jet stream of the Asian summer monsoon, *J. Clim.*, *17*, 1449–1458.

Knupp, K., R. Ware, D. Cimini, F. Vandenberghe, J. Vivekanandan, E. Westwater, and T. Coleman (2009), Ground-based passive microwave profiling during dynamic weather conditions, *J. Atmos. Oceanic Technol.*, *26*, 1057–1073.

Korak, S., K. Parameswaran, and C. S. Raju (2007), Tropospheric delay in microwave propagation for tropical atmosphere based on data from Indian subcontinent, *J. Atmos. Sol. Terr. Phys.*, *69*, 875–905.

Liou, Y. A., Y. T. Teng, T. V. Hove, and J. C. Liljegren (2001), Comparison of precipitable water observations in the near tropics by GPS, microwave radiometer, and radiosondes, *J. Appl. Meteorol.*, *40*, 5–15.

Malurkar, S. (1950), *Notes on Analysis of Weather of India and Neighbourhood*, Memoirs, vol. 34, India Meteorol. Dep., New Delhi.

Niell, A. E. (1996), Global mapping functions for the atmospheric delay at radio wavelengths, *J. Geophys. Res.*, *101*, 3227–3246, doi:10.1029/95JB03048.

Ohtani, R. (2001), Detection of water vapor variations driven by thermally induced local circulations using the Japanese continuous GPS array, *Geophys. Res. Lett.*, *28*, 151–154, doi:10.1029/2000GL011928.

Parameswaran, K., and B. V. K. Murthy (1990), Altitude profiles of tropospheric water vapor at low latitudes, *J. Appl. Meteorol.*, *29*(8), 665–679.

Pérez-Ramírez, D., D. N. Whiteman, A. Smirnov, H. Lyamani, B. N. Holben, R. Pinker, M. Andrade, and L. Alados-Arboledas (2014), Evaluation of AERONET precipitable water vapor versus microwave radiometry, GPS and radiosondes at ARM sites, *J. Geophys. Res. Atmos.*, *119*, 9596–9613, doi:10.1002/2014JD021730.

Pisharoty, P. R. (1965), Evaporation from the Arabian Sea and the Indian southwest monsoon, IMD, New Delhi, Bombay.

Pringent, C., W. B. Rossow, and E. Matthews (1997), Microwave land surface emissivities estimated from SSM/I observations, *J. Geophys. Res.*, *102*, 21,867–21,890, doi:10.1029/97JD01360.

Rajeevan, M., S. Gadgil, and J. Bhate (2010), Active and break spells of the Indian summer monsoon, *J. Earth Syst. Sci.*, *119*(3), 229–247.

Raju, C. S., K. Saha, B. V. Thampi, and K. Parameswaran (2007), Empirical model for mean temperature for Indian zone and estimation of precipitable water vapor from ground based GPS measurements, *Ann. Geophys.*, *25*, 1935–1948.

Raju, C. S., R. Renju, T. Antony, N. Mathew, and K. K. Moorthy (2013), Microwave radiometric observation of a waterspout over coastal Arabian sea, *IEEE Geosci. Remote Sens. Lett.*, *10*(5), 1075–1079.

Rocken, C., R. H. Ware, T. V. Hove, F. Solheim, C. Alber, and J. Johnson (1993), Sensing atmospheric water vapor with the Global Positioning System, *Geophys. Res. Lett.*, *20*, 2631–2634, doi:10.1029/93GL02935.

Rocken, C., T. V. Hove, J. Johnson, F. Solheim, M. Bevis, S. Chiswell, and S. Businger (1995), GPS sensing of atmospheric water vapor for meteorology, *J. Atmos. Oceanic Technol.*, *12*, 468–478.

Rogers, R. R., and A. P. Schwartz (1991), Mesoscale fluctuation of columnar water vapor, *J. Appl. Meteorol.*, *30*, 1305–1322.

Saha, K. R., and S. N. Bavadekar (1973), Water vapour bet and precipitation over the Arabian Sea during the northern summer, *Q. J. R. Meteorol. Soc.*, *99*, 273–278.

Simon, B., and P. C. Joshi (1994), Determination of moisture changes prior to the onset of south-west monsoon over Kerala using NOAA/TOVS satellite data, *Meteorol. Atmos. Phys.*, *53*, 223–231.

Smith, W. L. (1991), Atmospheric soundings from satellites—False expectation or the key to improved weather prediction, *Q. J. R. Meteorol. Soc.*, *117*, 267–297.

Solheim, F., J. R. Godwin, E. Westwater, Y. Han, S. J. Keihm, K. Marsh, and R. Ware (1998), Radiometric profiling of temperature, water vapor and cloud liquid water using various inversion methods, *Radio Sci.*, *33*, 130–134, doi:10.1029/97RS03656.

Sunilkumar, S. V., A. Babu, and K. Parameswaran (2013), Mean structure of the tropical tropopause and its variability over the Indian longitude sector, *Clim. Dyn.*, *40*, 1125–1140.

Tregoning, P., R. Boers, D. Brien, and M. Hendy (1998), Accuracy of absolute precipitable water vapor estimates from GPS observations, *J. Geophys. Res.*, *103*, 28,701–28,710, doi:10.1029/98JD02516.

Tyagi, A., A. B. Mazumdar, and D. S. Pai (2010), Monsoon 2010, *Rep.*, National Climate Centre Office of the Additional Director General of Meteorology (Research), Pune, India.

Wang, J., and L. Zhang (2007), Systematic errors in global radiosonde precipitable water data from comparisons with ground-based GPS measurements, *J. Clim.*, *21*, 2218–2238.

Ware, R. H., D. W. Fulker, S. A. Stein, D. N. Anderson, S. K. Avery, R. D. Clark, K. K. Droegemeier, J. P. Kuettner, J. B. Minster, and S. Sorooshian (2000), A real time national GPS network for atmospheric research and education, *Bull. Atmos. Meteorol. Soc.*, *81*, 677–694.

Xu, G., R. Ware, W. Zhang, G. Feng, K. Liao, and Y. Liu (2014), Effect of off-zenith observation on reducing the impact of precipitation on ground-based microwave radiometer measurement accuracy in Wuhan, *Atmos. Res.*, *140-141*, 85–94.